Pullback attractor crisis in a delay differential ENSO model

Chapter · January 2017

3 authors, including:

Mickael David Chekroun
University of California, Los Angeles

Michael Ghil
Ecole Normale Supérieure, Paris

Pullback attractor crisis in a delay differential ENSO model

Mickaël D. Chekroun, Michael Ghil, J. David Neelin

Abstract We study the pullback attractor (PBA) of a seasonally forced delay differential model for the El Niño–Southern Oscillation (ENSO); the model has two delays, associated with a positive and a negative feedback. The control parameter is the intensity of the positive feedback and the PBA undergoes a crisis that consists of a chaos-to-chaos transition. Since the PBA is dominated by chaotic behavior, we refer to it as a strange PBA. Both chaotic regimes correspond to an overlapping of resonances but the two differ by the properties of this overlapping. The crisis manifests itself by a brutal change not only in the size but also in the shape of the PBA. The change is associated with the sudden disappearance of the most extreme warm (El Niño) and cold (La Niña) events, as one crosses the critical parameter value from below. The analysis reveals that regions of the strange PBA that survive the crisis are those populated by the most probable states of the system. These regions are those that exhibit robust foldings with respect to perturbations. The effect of noise on this phase-and-paramater space behavior is then discussed. It is shown that the chaos-to-chaos crisis may or may not survive the addition of small noise to the evolution equation, depending on how the noise enters the latter.

Mickaël D. Chekroun
Department of Atmospheric and Oceanic Sciences, University of California, Los Angeles, U.S.A, e-mail: mchekroun@atmos.ucla.edu

Michael Ghil
Geosciences Department, Ecole Normale Supérieure and PSL Research University, Paris, France, and Department of Atmospheric and Oceanic Sciences, University of California, Los Angeles, U.S.A, e-mail: ghil@atmos.ucla.edu

J. David Neelin
Department of Atmospheric and Oceanic Sciences, University of California, Los Angeles, U.S.A, e-mail: neelin@atmos.ucla.edu

1 Introduction and motivation

The El Niño–Southern Oscillation (ENSO) is a dominant mode of climate variability on seasonal-to-interannual time scales and affects the climate over a great portion of the globe on interdecadal and longer time scales. A major aspect of ENSO is the strong coupling between the Tropical Pacific ocean and the atmosphere above, and the physical mechanisms that give rise to ENSO are fairly well understood [NBH$^+$98, Phi92].

A key mechanism, originally proposed in [Bje69], is the positive atmospheric feedback on the equatorial sea surface temperature (SST) field via the surface wind stress. Still, ENSO's unstable, recurrent but irregular behavior implies challenges for prediction [Can86], even at subannual lead times. Conceptual numerical modeling plays a prominent role in understanding ENSO variability and developing prediction methods for it [GJ98, NBH$^+$98, MNY03, CKG11]. The delayed oscillator description of ENSO has led to a hierarchy of models of increasing complexity that include delay effects taking various forms [SS88, BH89, NBH$^+$98, GT00], via negative [GZT08, GZ15] and positive [TSCJ94] feedbacks.

Seasonal forcing has been suggested as a crucial ingredient in explaining ENSO's irregularity [JNG94, TSCJ94, JGN95, TCZ95, JNG96]. In this approach, the intrinsic ENSO oscillator may enter into nonlinear resonance with the seasonal forcing. In the case of exact frequency locking with the seasonal cycle, such resonant behavior is characterized by perfect periodicity. ENSO's irregularity occurs when the nonlinear effects are stronger, and several resonances may coexist. In this case, the ENSO oscillator is not able to lock to a single resonance, and it jumps irregularly between several resonances, while the resulting irregular behavior still bears the fingerprint of the underlying frequency-locked regimes that now co-exist. Dynamically, this phenomenon corresponds to the overlapping of nonlinear resonances also known as Arnold tongues in parameter space [JBB84, Arn88, GCS08]. Noise due to atmospheric internal variability has also been shown to be an important factor in ENSO irregularity [BNG97, EL97, KM97].

To study the effects of the seasonal cycle in the aforementioned ENSO models, direct numerical integrations and examination of return maps in a low-dimensional, reconstructed phase space[1] are often preferred to a rigorous mathematical analysis, which is typically challenging to carry out. Recently, continuation methods for bifurcations in delay differential equations (DDEs) have also been used to analyze the interactions of the seasonal cycle with the ENSO oscillator [KS14, KKP15, KKP16]. Rigorous approximation techniques of DDEs by systems of ordinary differential equations (ODEs) [CGLW16] offer another path to the analysis of such interactions.

In this study, we propose yet another approach, which relies on the theory of pullback attractors (PBAs) [CSG11, CLR13] and the statistical equilibria they support [CGH12, LR14]. The application to DDEs herein uses careful numerical approximations of the PBAs [CSG11], along with visualization in low-dimensional, embedded

[1] Relying, for instance, on the Takens embedding theorem [Tak81].

phase space; see [GZ15, Ghi17] for preliminary DDE results. Here, PBAs are used to analyze a complicated chaos-to-chaos transition.

We focus in this chapter on the seasonally forced ENSO model of [TSCJ94] that includes delayed positive and negative feedback mechanisms. For the sake of the nonspecialist reader, this model is outlined in Sect. 2.1 below. We compute for this model approximations of the PBA and of the statistical equilibrium it supports, both of which are represented in a natural two-dimensional (2-D) embedded phase space. Recall that, loosely speaking, a global PBA $\mathscr{A}(t)$ describes the states in the system's phase space X that are reached at a time t, when the system is initiated from an asymptotic past, $s \to -\infty$, and the initial states are varied within a collection of bounded sets of X [CLR13]. The statistical equilibrium μ_t supported by the PBA, as defined in Sect. 2.4, is crucial for the description of the distribution of current states at time t [Rue99, CSG11].

After recalling in Sect. 2.2 some fundamentals about PBAs, in particular in the context of DDEs, we first numerically show the "strangeness" of an embedded version of $\mathscr{A}(t)$ in Sect. 2.3.1. In particular, the folding and stretching that is typical of nonlinear, chaotic dynamics in the autonomous setting are observed in various regions of this PBA. After proving the periodicity of $\mathscr{A}(t)$ with the same period as that of the seasonal forcing, the time evolution of $\mathscr{A}(t)$ within a calendar year is then analyzed in Sect. 2.3.2. There, we show that the PBA provides a natural global geometric view of the dynamics, consistent with variations in ENSO phase-locking that occur within a given frequency-locked regime, as previously documented in the literature [NJS00, GT00]. In Sect. 2.4, we provide a brief but still rigorous description of the aforementioned statistical equilibrium μ_t.

Section 3 contains a parameter-dependence study of the PBA $\mathscr{A}(t)$ and of the statistical equilibrium μ_t it supports. Numerical experiments allow us to conclude that a chaos-to-chaos crisis takes place as the intensity of the positive feedback crosses a critical value; see Sect. 3.1. The crisis separates two different types of overlapping of nonlinear resonances. In Sect. 3.2, we analyze the changes in the PBA and in the statistical equilibrium across the crisis. Both these mathematical objects change relatively smoothly, until reaching eventually an abrupt, discontinuous change as the critical parameter value is crossed. The crisis manifests itself by a brutal change not only in the size but also in the shape of the PBA, which keeps its strange character across the transition.

Dynamically, this abrupt change in the PBA is associated with the sudden disappearance of extreme warm (El Niño) and cold (La Niña) events, as one crosses the critical parameter value from below. The analysis of the statistical equilibrium μ_t supported by the PBA $\mathscr{A}(t)$ reveals that the regions of the strange PBA that survive the crisis are those populated by the most probable states of the system. These regions are those that exhibit robust foldings with respect to perturbations.

Two dynamical mechanisms are proposed in Sect. 3.3 to explain the origin of the chaos-to-chaos crisis identified herein. One consists of the crossing of a crisis line within an overlapping region of two Arnold tongues [MK13] that separate two co-existing PBAs. The other consists of a PBA-widening scenario suggested in [GORY87] for low-dimensional autonomous maps. In our case, an unstable pullback periodic orbit would collide with $\mathscr{A}(t)$ as one crosses a critical value of the control parameter, causing the PBA widening reported hereafter.

Finally, the effect of noise on this phase-and-parameter space behavior is discussed in Sect. 3.4. It is shown that the chaos-to-chaos crisis may or may not survive the addition of small noise to the evolution equation, depending on how the noise enters the latter. These noise effects find a natural interpretation within each of the aforementioned possible crisis mechanisms.

2 PBAs and statistical equilibria in a periodically forced ENSO model with delays

2.1 The model

We focus hereafter on the nonlinear delay oscillator mechanism, and analyze a statistical crisis occurring in this model as a certain control parameter varies. The model takes its root in the following conceptual description.

A positive SST perturbation along the eastern equatorial Pacific weakens the easterly trade winds above the equator. The change in the winds excites a downwelling wave in the thermocline that travels eastward to the South American coast as equatorial Kelvin waves and an upwelling signal that travels westward as equatorial Rossby waves. The downwelling Kelvin waves enhance the warming off the coast of South America, starting an El Niño event. Subsequently, the westward-traveling upwelling Rossby waves are reflected from the western boundary of the Pacific Ocean as upwelling Kelvin waves, which travel eastward to counter the downwelling Kelvin waves. This negative feedback ultimately terminates the El Niño event.

A simple model of such a delay mechanism, including one Kelvin wave, one Rossby wave mode, and a dynamic link from mid-Pacific wind stress anomalies to these equatorial wave modes has been proposed in [TSCJ94]. The model includes an idealized seasonal forcing term that represents the effects of the numerous seasonally varying features of the equatorial Pacific ocean and atmosphere, such as wind amplitude and SST variations. The single dependent variable in the equation is $h(t)$—the thermocline depth deviation from seasonal depth values at the eastern boundary—and the model reads as follows

$$\frac{dh}{dt} = aR\Big[h\Big(t - \frac{L}{2C_K}\Big)\Big] - bR\Big[h\Big(t - \frac{L}{C_K} - \frac{L}{2C_R}\Big)\Big] + c\cos(\omega_a t + \varphi). \qquad (1)$$

A version of this model with only the negative feedback included was studied in [GZ15], including its PBA.

In Eq. (1) L is the basin width, ω_a denotes the annual frequency of the seasonal forcing, and φ denotes its phase. The wind-forced Kelvin mode that travels eastward at a speed C_K is represented by the first term in the right-hand side of Eq. (1). It takes this wave a time $L/(2C_K)$ to reach the eastern boundary from the middle of the basin.

The second term is due to the Rossby wave that travels westward at a speed C_R; this wave is excited by the wind at a delayed time, namely $t-(L/C_K+L/(2C_R))$, and it is reflected as a Kelvin wave off the western basin boundary.

The function $R[h]$ relates wind stress to SST, and SST to thermocline depth. We follow here [MCZ91], where the nonlinear form of $R[h]$ is given by

$$R[h]=\begin{cases} b_+ + \frac{b_+}{a_+}\Big(\tanh\big(\frac{\kappa a_+}{b_+}(h-h_+)\big)-1\Big), & \text{if } h_+<h,\\ \kappa h, & \text{if } h_-\le h\le h_+,\\ -b_- - \frac{b_-}{a_-}\Big(\tanh\big(\frac{\kappa a_-}{b_-}(h-h_-)\big)-1\Big), & \text{if } h<h_-. \end{cases} \tag{2}$$

The specific form of $R[h]$ reflects the non-uniform stratification of the ocean; it is fashioned after the shape of the tropical thermocline. The slope of $R(h)$ at $h=0$, set by the parameter κ, provides a measure of the strength of the ocean-atmosphere coupling. Based on [MCZ91], we consider here $a_\pm>1$, and

$$h_+=\frac{b_+}{\kappa a_+}(a_+-1), \quad h_-=-\frac{b_-}{\kappa a_-}(a_--1). \tag{3}$$

These values ensure that $R[h]$ is continuous at h_+ and h_-. As $h\to\pm\infty$, we get $R[h]\to b_\pm$. The parameters $a_\pm$ control the curvature of $R[h]$, and the greater $a_\pm$, the faster the limits $b_\pm$ are reached as $h\to\pm\infty$. The values used in our numerical simulations are reported in Table 1 below.

Table 1: Glossary of model's parameter

Parameter	Interpretation	Numerical value
L	basin width	1
ω_a	frequency of the annual cycle	$2\pi/360$
φ	phase of the forcing	$\pi/2$
C_K	Kelvin wave speed	$1/69$ days^{-1}
C_R	Rossby wave speed	$1/207$ days^{-1}
$a_{+/-}$	Control parameters of the curvature of $A[h]$	1
b_-	limit of $A[h]$ as $h\to-\infty$	-0.44
b_+	limit of $A[h]$ as $h\to+\infty$	2.2
a,b	magnitude of the feedbacks	$a=(1.12+\delta)/180$, $b=1/120$
c	magnitude of the periodic forcing	c=2.2/180
κ	slope at the origin in Eq. (2)	2.6

The parameter κ, cf. [TSCJ94, Fig. 1], is a key parameter in the control of the model's dynamical behavior. For small values of κ, the time series $h(t)$ is, for instance, perfectly periodic with the annual period of the forcing. Besides this simple periodic behavior, three dynamical regimes are typically exhibited by the model. For the parameter values used in [TSCJ94], these regimes are classified as follows.

(I) Irregular quasi-periodic dynamics. As κ increases, an internal frequency ω_i appears; it characterizes the natural oscillator of the Tropical Pacific's ocean-atmosphere system [JN93, NBH+98]. This second frequency is, in general, incommensurable with the annual frequency; the superposition of two incommensurable frequencies creates a quasi-periodic time series. The resulting oscillations are irregular but not chaotic; the power spectrum shows two dominant frequencies with several subharmonics; see again [TSCJ94, Fig. 1].

(II) Frequency-locked dynamics. For a steeper slope of $A[h]$ at $h = 0$, the system becomes frequency-locked: The frequency of the nonlinear delay oscillator changes slightly to a simple rational multiple of the driving annual frequency: $\omega_i = \omega_a p/q$, with p and q integers. This regime corresponds to a nonlinear resonance between the driving annual frequency ω_a and the internal oscillatory frequency ω_i. The time series is periodic, and the phase-space diagram (in a Poincaré section) is a set of points whose number depends on the values of p and q. The parameter regimes corresponding to the frequency-locked solutions are also known as Arnold tongues; see, for instance, [GCS08, Fig. 7].

(III) Chaos by overlapping of resonances. For certain values of κ, the time series $h(t)$ becomes irregular, and it is associated with a strange PBA and a power spectrum that is broad and no longer contains sharp peaks, as in Regimes (I) or (II). Two or more frequency-locked solutions—that is, solutions with different ratios p/q—may coexist; the nonlinear resonances are said to overlap in this case. The chaotic behavior is caused by the irregular "trapping" of the system among the different possible resonances. This characterization of Regime (III) in terms of a strange PBA is provided in Sec. 2.2 below.

In what follows, we denote by τ_1 and τ_2, the basin-crossing times $L/(2C_K)$ and $L/C_K + L/(2C_R)$, respectively.

2.2 PBAs of delay models with time-dependent forcing

Recall that the standard theory of global attractors in the autonomous case [Tem97] requires one first to define a phase space in which the solutions of a given evolution equation are well-defined. It is necessary to proceed in the same way for non-autonomous dynamical systems (NDSs) and their PBAs.

In the case of nonlinear DDEs, such as Eq. (1), several function spaces can be used as a state space. Among the most standard ones, those that start with the space of continuous functions on the interval $[-\tau, 0]$ play an important role; see, for instance, [DvGVLW95, HVL93]. Hilbert spaces, though, are better adapted to the approximation of DDEs by systems of ordinary differential equations (ODEs) [CGLW16].

The reformulation of Eq. (1) as a retarded functional differential equation (RFDE) is classical and proceeds as follows. Let us denote by h_t the time evolution of the history segments of a solution h to Eq. (1). In other words, for each t, h_t is a function from $[-\tau,0]$ into $\mathbb{R}$ defined as

$$h_t(\theta) := h(t+\theta), \qquad t \geq 0, \qquad \theta \in [-\tau, 0]. \tag{4}$$

Introducing the phase space $X := \mathscr{C}([-\tau,0],\mathbb{R})$ of continuous functions from $[-\tau,0]$ into $\mathbb{R}$, with $\tau = \tau_2 > \tau_1$, and the nonlinearity $\mathscr{F}$ defined for all ψ in X by

$$\mathscr{F}(\psi) = aR\left[\psi(-\tau_1)\right] - bR\left[\psi(-\tau_2)\right], \text{ with } R \text{ given in (2)}, \tag{5}$$

Eq. (1) can be recast into the following RFDE

$$\frac{\mathrm{d}h}{\mathrm{d}t} = \mathscr{F}(h_t) + g(t), \tag{6}$$

in which the time-dependent forcing $g(t)$ is given by

$$g(t) = c\cos(\omega t). \tag{7}$$

Note that he nonlinearity $\mathscr{F}$ in (5) is bounded as a mapping from X into $\mathbb{R}$,

$$|\mathscr{F}(\psi)| \leq \max(b_+, |b_-|), \text{ for all } \psi \text{ in } X. \tag{8}$$

Furthermore, $\mathscr{F}$ is globally Lipschitz on X endowed with the uniform-norm topology, i.e. the topology induced by the supremum norm

$$\|\phi\|_\infty := \sup_{\theta \in [-\tau,0]} |\phi(\theta)|. \tag{9}$$

Since $\mathscr{F}$ is continuous, due to Eqs. (3), as well as bounded and Lipschitz continuous, the general theory of RFDEs [HVL93] applied to Eq. (6) ensures that, for any (s,ϕ) in $\mathbb{R}\times X$, there exists a unique solution to Eq. (6), defined on a maximal interval $[s, T_{\max}(\phi))$, $T_{\max}(\phi) > s$, such that

$$h_s(\theta) = \phi(\theta), \;\; \theta \in [-\tau, 0]. \tag{10}$$

Moreover if $T_{\max}(\phi) < \infty$, then the solution blows up at time $T_{\max}(\phi)$, i.e.

$$\lim_{t \to T_{\max}(\phi)^-} \|h_t\|_\infty = \infty, \tag{11}$$

On the other hand, an integration of Eq. (6) between s and t for $s \leq t < T_{\max}(\phi)$ and the bounds (8) with $g(t) \leq c$, lead to the estimate

$$\|h_t\|_\infty \leq \|\phi\|_\infty + (T_{\max}(\phi) - s)(c + \max(b_+, |b_-|)). \tag{12}$$

This latter inequality is incompatible with (11) and therefore $T_{\max}(\phi) = \infty$ for all ϕ in X. As a consequence, solutions to Eq. (6) are guaranteed to exist in X for all positive times t, and to be uniquely determined by an initial history ϕ in X, taken over any anterior time interval $[s-\tau, s]$, with $s \leq t$.

In other words, one can define a nonlinear process [HVL93, Chap. 4], i.e. a solution map U defined by

$$(t, s, \phi) \mapsto U(t, s)\phi := h_t \in X,\ t \geq s,\ \phi \in X, \tag{13}$$

where h_t denotes the unique solution to Eq. (6) that emanates from ϕ at a time $s \leq t$, i.e. such that $h_s = \phi$. The existence and uniqueness property translates here into the process composition property, which replaces the more traditional (semi-)group property [Tem97, Chap. I, Sec. 1.1] and is formulated here as

$$U(t, s) \circ U(s, r) = U(t, r),\ \ t \geq s \geq r. \tag{14}$$

The solution map U can be thus referred to as a two-parameter semi-group of transformations of X. It provides a two-time description of the dynamics associated with Eq. (1): the time s describes when the system was initialized, while the other time t is associated with the current state of the system. In the autonomous case, only the amount of time separating s and t, i.e. $t-s$, matters and a one-parameter (semi-)group suffices to entirely determine the dynamics; e.g. [CSG11, CGLW16]. In the non-autonomous case, the history of the forcing between the time s and the time t — which we call a forcing snippet — is an important ingredient of the dynamics and may drive the system differently between a time s' and a time t', even though $t'-s' = t-s$.[2]

Note also that the phase space X on which the process U is acting is infinite-dimensional as a function space. Even in this setting, a PBA can be rigorously defined [CMRV05, CLR13]. A family of compact[3] sets $\{\mathscr{A}(t)\}$ of X is then said to be a (global) PBA for U, if it satisfies

(i) (Invariance property) $U(t, s)\mathscr{A}(s) = \mathscr{A}(t)$ for all $t \geq s$; and
(ii) (Pullback attraction property) $\lim_{s\to-\infty} \mathrm{dist}_X(U(t, s)B, \mathscr{A}(t)) = 0$, for all bounded subsets B of X.

The pullback attraction property (ii) considers a collection of states of the system at time t when the system is initiated in a distant past s, as s goes to $-\infty$ and for initial states lying in B. As B is varied in the collection of bounded subsets of X, a useful explicit PBA characterization in terms of the omega limit set is available [CLR13, Theorem 2.12]; see also (18) below.

Note that $\mathrm{dist}_X(E, F)$ denotes here the Hausdorff semi-distance between the subsets E and F of X,

$$d_X(E, F) := \sup_{x\in E} d_X(x, F) \text{ with } d_X(x, F) := \inf_{y\in F} \|x - y\|. \tag{15}$$

[2] Still, a segment $[s', t']$ of the forcing may drive the system in a way that is similar to that over the segment $[s, t]$, even when $g(t)$ is a white noise, provided the system's solutions exhibit recurrent patterns as time evolves; see [CKG11, KCRG13].

[3] Here compact set is understood in the sense of point set topology [Kel75].

One calls $d_X(E,F)$ a semi-distance since, in general, $d_X(E,F) \neq d_X(F,E)$ and $d_X(E,F) = 0$ merely implies $E \subset F$. From (ii) above, one can thus say, loosely speaking, that, for any set B of initial data, $U(t,s)B$ is "almost included" in the pullback attractor $\mathscr{A}(t)$, whenever $t-s$ is sufficiently large. Intuitively, for B spanning a sufficiently large ensemble of possible initial data, one can reasonably say that $U(t,s)B$ constitutes a good approximation of a significant portion of the pullback attractor $\mathscr{A}(t)$.

In the nonlinear physics literature, $U(t,s)B$ is often called a "snapshot attractor" [RGO90, BKT11, BT12, BKT13, DBT15]. In practice one lets, roughly speaking, a cloud of points — each driven by the same segment of the forcing — flow forward in time. However, to justify this procedure, one needs to ensure the existence of a global PBA, which allows for a rigorous characterization of dissipation in the presence of time-dependent forcing, either deterministic [CLR13] or random [CF94, CDF97]. This rigorous treatment has to be valid also in the infinite-dimensional context of partial differential equations (PDEs), such as the 2-D Navier-Stokes equations, subject to time-dependent disturbances, or to that of the delay differential ENSO model considered here. Remarkably, global PBAs support meaningful invariant measures that characterize the statistics of the nonlinear, non-autonomous dynamics, as explained in Section 2.4 below. Global PBAs are thus natural objects to describe both the statistics and the geometry of non-autonomous dynamics, and identifying conditions for their existence is theoretically crucial.

Useful conditions—expressing often a form of balance between the forcing and the intrinsic dissipative effects of the underlying autonomous dynamics—may be identified within the PBA framework to ensure their existence; see, for instance, [PGC16, Appendix] and the proof of [KCG15, Theorem 3.1]. In the context of the DDE model (6), the nonlinearity $\mathscr{F}$ defined in (5) is responsible for autonomous dissipative effects in X and the periodic forcing $g(t)$ permits their translation into a pullback dissipation.

We do not address the rigorous existence of such a pullback dissipation here, nor of a global PBA, and refer to [CLR01, CMRV05] for techniques to prove the existence of PBAs for DDEs. Instead, we illustrate next, by means of numerical simulations, geometric features of the global PBA associated with Eq. (6). These features are studied in the chaotic regime that corresponds to the value $\delta = 15 \times 10^{-3}$ of the parameter δ that affects the magnitude of the feedback a in the model (1), while the other parameters take the values listed in Table 1.

2.3 A strange PBA and its time evolution

2.3.1 Characterizing strangeness of a PBA

To analyze the structure of the global PBA for the parameters considered in this chapter, we first computed approximations of the PBAs $\mathscr{A}(t)$ for different values of t and for $\delta = 15 \times 10^{-3}$. To do so, we have integrated numerically Eq. (1), using a set

B of $N = 5 \times 10^5$ initial histories ϕ that have been sampled over $[-\tau, 0]$, according to a distribution described in Sec. 3.2, below. The results are shown in Fig. 1 for $t-s$ sufficiently large: we found that $t \approx 147.64$ yr and $s = 0$ are sufficient to ensure convergence, that is to have $U(t,t-s)B$, with $\phi \in B$, "quasi-contained" in $\mathscr{A}(t)$, i.e. $\mathrm{dist}_X(U(t,t-s)B, \mathscr{A}(t)) \approx 0$. Thus we do not distinguish $U(t,t-s)B$ from $\mathscr{A}(t)$ in the discussion below.

The PBA $\mathscr{A}(t)$ is plotted in Fig. 1 in the embedded phase space of the delay coordinates $(h(t), h(t+1))$, where the unit delay corresponds to 1 year. The PBA's global structure is indicative of nonlinear effects, with characteristic folds occurring in several locations. To simplify the discussion, we often make hereafter no distinction between $\mathscr{A}(t)$ and its embeddings, such as that shown in this figure. A zoom at a specific location of $\mathscr{A}(t)$, depicted in the inset of Fig. 1, shows finer structure with several interleaved stretchings and foldings that occur over a very narrow region of the embedded phase space. Several other regions of the PBA (not shown) reveal the same fine filamentation when put under this kind of magnifying glass.

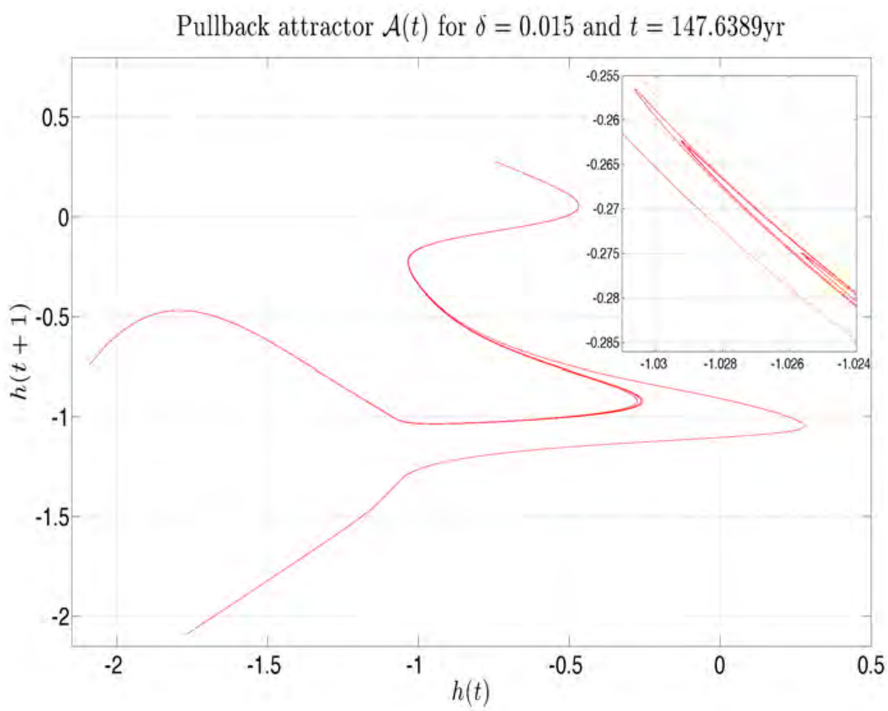

Fig. 1: **A strange pullback attractor (PBA) $\mathscr{A}(t)$ associated with the periodically forced delay differential equation (DDE) (1).** The PBA is projected onto the delay coordinates $(h(t), h(t+1))$.

It is, in fact, not surprising to find a complex structure associated with stretching and folding in the global PBA of a system exhibiting chaos when subject to a time-dependent forcing: such PBA geometry was illustrated in [CSG11, PGC16] for dynamical systems of lower dimension than considered here; see also [Ghi17]. The emergence of strange attractors in periodically forced dynamical systems has even been addressed rigorously recently for a broad class of evolution equations, including some parabolic PDEs [LWY13]. At the core of this approach is a geometric mechanism for the production of chaos that has been first identified in [WY08] and generalized in subsequent works of the same authors [WY01, WY03]. In particular [WY03, Theorem 1] shows that when suitably kicked by an external periodic forcing, a limit cycle can be turned into a strange attractor. Further details of this theory are discussed below in Sec. 2.4. We turn next to the PBA's time evolution.

2.3.2 Time evolution of the PBA

First, note that, due to the periodicity of the forcing, the process U is T-periodic, with $T = 1$ yr. Indeed, given $s < t$, it follows that integrating Eq. (6) from $s+T$ to $t+T$ is equivalent to integrating it from s to t, since the vector field $\mathscr{F}$ (on X) is time independent and g is T-periodic. In other words, for all ϕ in X and any $s \leq t$,

$$U(t+T,s+T)\phi = U(t,s)\phi. \tag{16}$$

From this property we conclude that the pullback omega limit set of any bounded subset B of X [CLR13, Definition 2.2] satisfies[4]

$$\omega_B(t) := \bigcap_{\tau\geq 0} \overline{\bigcup_{s\geq\tau} U(t,t-s)B} = \bigcap_{\tau\geq 0} \overline{\bigcup_{s\geq\tau} U(t+T,t+T-s)B} = \omega_B(t+T), \tag{17}$$

where $\overline{E}$ ($E \subset X$) denotes the set of points of X that can be obtained as limit of elements in E. Thus, recalling the characterization of the global PBA in terms of omega limit sets [CLR13, Theorem 2.12], we have

$$\mathscr{A}(t) := \overline{\bigcup_{B\in\mathscr{B}(X)} \omega_B(t)} = \overline{\bigcup_{B\in\mathscr{B}(X)} \omega_B(t+T)} = \mathscr{A}(t+T), \text{ for all } t \in \mathbb{R}, \tag{18}$$

where $\mathscr{B}(X)$ denotes the collection of bounded subsets of X.

The time evolution of $\mathscr{A}(t)$ within a year is illustrated in Fig. 2; the four snapshots are shown at 3-month intervals. The periodicity of the global PBA can be seen by comparing the bottom snapshot in Fig. 2 (red curve) for $t \approx 146.64$ yr with the PBA shown in Fig. 1 for $t \approx 147.64$ yr.

As can be seen in Fig. 2, the PBA is experiencing global deformations and shifts with time in the embedded phase space. The PBA's strangeness, with its foldings and

[4] This set is equivalently defined as the set of elements ψ in X obtained as the pullback limit $\psi = \lim_{k\to\infty} U(t,s_k)\phi_k$, with $s_k \to -\infty$ and $\phi_k \in B$.

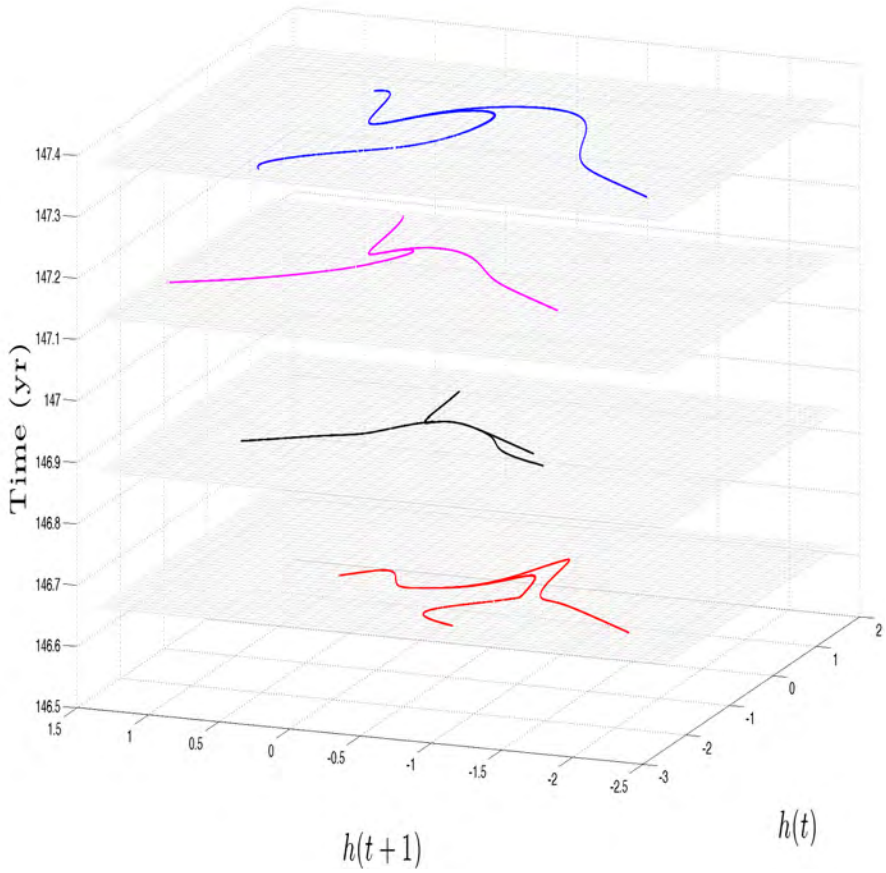

Fig. 2: **Time evolution of the PBA $\mathscr{A}(t)$ in Fig. 1 throughout a calendar year.** Each snapshot is represented — for $\delta = 15 \times 10^{-2}$ — by a heavy curve, hiding the fine-scale details and foldings shown in Fig. 1 for $t \approx 147.64$. Note that the snapshot of $\mathscr{A}(t)$ that is represented in red at the bottom of the figure for $t \approx 146.64$ yr is actually exactly the same as that shown in Fig. 1, due to the periodicity of the seasonal forcing; see (18).

stretchings, is also present in each of the snapshots shown in Fig. 2, but the mode of representation adopted here prevents one to display these fine-scale structures.[5]

As we will see in the next section, each PBA $\mathscr{A}(t)$ supports a complicated probability measure that describes the statistics of the dynamics and, in particular, that of the model's extremes events. The latter correspond to the PBA's filaments that meander with time in the embedded phase space. This meandering helps provide a useful physical interpretation of the model's dynamics.

[5] Heavy curves have been used for a better visualization of the overall evolution in the three-dimensional representation used in Fig. 2.

For instance, due to the embedding used, at constant time, for each of the horizontal planes shown in Fig. 2, one can infer that a negative and large value of $h(t)$ followed by a negative and large value of $h(t+1)$, i.e. one year later, is less likely to occur in boreal winter (black and magenta curves in Fig. 2) than in boreal summer (blue and red curves in Fig. 2). This seasonal dependence of the extremes is well-known in ENSO models, and it is reflected strikingly here by the global PBA's time evolution.

We turn next to a natural class of probability measures supported by a strange PBA, such as the one shown in Fig. 1. These invariant measures will help complete our description of seasonal dependence of the extremes, as encoded by the time evolution of $\mathscr{A}(t)$, by attributing useful statistics to this dependence.

2.4 Pullback statistical equilibria of periodically forced systems

In this section, we provide the theoretical underpinnings for the study of probability measures in periodically forced, infinite-dimensional systems like our ENSO model. Given a reference probability measure $\mathfrak{m}_0$ on the phase space X, one wishes to consider time-dependent probability measures μ_t on X that can be obtained as a weak limit of the measure $\mathfrak{m}_t := U(t,s) * \mathfrak{m}_0$, as $s \to -\infty$.

Equivalently, the probability measure $\mathfrak{m}_t$ is defined for any Borel set E of X by

$$\mathfrak{m}_t(E) = \mathfrak{m}_0(U(t,s)^{-1}(E)), \tag{19}$$

i.e. it gives the "$\mathfrak{m}_0$-volume" of points of X that fall into the set E when propagated by $U(t,s)$, and it characterizes therewith the evolution of the initial measure $\mathfrak{m}_0$ under the action of $U(t,s)$. A weak limit is understood here in the following sense: for all continuous and bounded real-valued function φ on X, we have

$$\lim_{s \to -\infty} \int_X \varphi(U(t,s)x)\, \mathrm{d}\mathfrak{m}_0(x) = \int_X \varphi(x)\, \mathrm{d}\mu_t(x). \tag{20}$$

In infinite dimensions, though, the existence of the limit on the left-hand side of (20) is not guaranteed in general, even in the autonomous case. By making, however, use of a generalized Banach limit[6] [FMRT01], a weaker version of (20) has been shown to hold in the autonomous setting[7] for a broad class of infinite-dimensional dissipative systems, as soon as they exhibit a global attractor; see [CGH12, Theorem 2.2].

This result has been generalized to the non-autonomous setting by [LR14]. In either case, autonomous or not, [CGH12, Theorem 2.2] or [LR14, Theorem 4.1] ensures that such a limiting measure is necessarily invariant and supported by the global attractor. In the non-autonomous setting, the invariance property is

[6] Allowing, for instance, for a weighted combination over the possible accumulation points in X of the trajectory $s \mapsto U(t,s)x$.

[7] In this case, $U(t,s) = S(t-s)$ becomes a (semi-)flow and μ_t is time independent.

$$U(t,s) * \mu_s = \mu_t, \tag{21}$$

or, equivalently,

$$\int_{\mathscr{A}(s)} \varphi(U(t,s)x)\,\mathrm{d}\mu_s(x) = \int_{\mathscr{A}(t)} \varphi(x)\,\mathrm{d}\mu_t(x), \;\; s \le t, \;\; \varphi \in C_b(X), \tag{22}$$

with $C_b(X)$ the space of real-valued, continuous and bounded functions on X.

In the periodically forced case of Eq. (6), the existence of a global PBA $\mathscr{A}(t)$ ensures thus that, starting from an initial probability measure $\mathfrak{m}_0$, an invariant measure μ_t supported by $\mathscr{A}(t)$ is reached at time t under the action of $U(t,s)$, as the initial time s is stretched into the past. Furthermore, recalling that $\mathscr{A}(t) = \mathscr{A}(t+T)$, cf. (18), one can prove from (21) and (16) that

$$\mu_{t+T} = \mu_t, \;\; \text{with } T = 1 \text{ yr}. \tag{23}$$

Obviously, the existence of a unique invariant probability measure μ_t that satisfies Eq. (20)—irrespectively of $\mathfrak{m}_0$—is not yet guaranteed at this stage. The difficulty does not come from the techniques underlying the aforementioned mathematical results, but rather from the infinite-dimensional nature of the phase space X. In finite dimensions, a unique measure μ_t satisfying (20), irrespective of any measure $\mathfrak{m}_0$ possessing a density with respect to the Lebesgue measure, has been shown to exist for several systems [ER85, Rue99], giving rise often to a Sinai-Ruelle-Bowen (SRB) measure. In the non-autonomous setting, this measure describes the statistics of time evolutions of almost all solutions starting from the basin of attraction of a PBA $\mathscr{A}(t)$; see [Rue99, CSG11, You16].

There is, however, no direct generalization of the ideas surrounding SRB measures to infinite dimensions. This is due in part[8] to the absence of a notion of Lebesgue measure in function spaces such as X.

As mentioned earlier in Sect. 2.3, an important step towards the existence of an analogue of SRB measures in infinite dimension has been taken; see [You16] for a recent survey. It concerns the case of periodically forced systems that exhibit a limit cycle when the forcing is turned off. Loosely speaking, in the case of the origin losing its stability via a supercritical Hopf bifurcation, if the strong stable foliation W^{ss} originating from 0 — and for which each W^{ss}-curve meets the limit cycle in exactly one point — has W^{ss}-curves twisted near the origin, then suitable periodic kicks in the vicinity of the supercritical limit cycle lead to folding and stretching of the phase space, and eventually to a strange attractor.

If the foliation is of finite codimension and sufficiently regular, e.g. Lipschitz continuous, then there is a well-defined Lebesgue measure class transversal to its leaves. If the codimension is two, for instance, and — for every embedded 2-D surface S transversal to the leaves of W^{ss} — a given property holds almost every-

[8] The other aspect of the problem that renders the analysis difficult is tied to the lack of smoothing of the flow in probability space by the Liouville equation [CNK+14]— in the present, deterministic setting — as compared to the Fokker-Planck equation, which is its counterpart in the presence of noise; see [CTDN16].

where with respect to the Riemannian measure on S, then it holds almost everywhere transversal to W^{ss}. This way, a proper Lebesgue-like meaning to “almost all solutions” can be given, and the conclusion of [LWY13, Theorem 3.4] ensures the existence of SRB measures for a broad class of periodically kicked evolution equations in infinite dimension, whenever the kicks are suitable and the twist of the W^{ss}-curves sufficiently strong.

Such a theory of SRB measures provides a very useful and general geometric mechanism for the production of chaos from periodically kicked evolution equations, but its application to Eq. (6) requires a certain level of mathematical technicalities that go beyond the scope of this article. Instead, we will show in Sec. 3.2, by means of high-resolution numerics, that the singular nature of a statistical equilibrium μ_t satisfying (20), for an appropriately chosen initial probability measure $\mathfrak{m}_0$, strongly suggests the existence of such an SRB measure for Eq. (6), albeit without guaranteeing its uniqueness.

3 Chaos-to-chaos crisis and pullback symptoms

3.1 Crisis symptoms in the Kolmogorov-Smirnov metric

For simplicity, let us consider probability measures ρ and ν on the real line $\mathbb{R}$. We introduce the following abstract probability metric, subject to the choice of a set $\mathscr{F}$ of test functions:

$$d_{\mathscr{F}}(\rho,\nu) = \sup_{f\in\mathscr{F}}\left|\int f\,\mathrm{d}\rho - \int f\,\mathrm{d}\nu\right|. \tag{24}$$

If $\mathscr{F} = \{f : \|f\|_\infty \leq 1\}$ then $d_{\mathscr{F}}$ is the total variation metric TV. If

$$\mathscr{F} = \{\mathbb{1}_{(-\infty,x]},\, x\in\mathbb{R}\}, \tag{25}$$

then $d_{\mathscr{F}}$ is the Kolmogorov-Smirnov (KS) metric d_{KS}.

It follows readily that, for any pair (ρ,ν) of probability measures,

$$d_{\mathrm{KS}}(\rho,\nu) \leq TV(\rho,\nu). \tag{26}$$

If one considers a family $\{\rho_\lambda\}$ of probability measures indexed by a parameter λ, a key property of the KS metric is that a discontinuity of the mapping $\lambda \mapsto d_{\mathrm{KS}}(\rho_{\lambda_0},\rho_\lambda)$ at a point $\lambda = \lambda_*$ indicates a brutal change in the cumulative distribution function (CDF) of ρ_λ at that point. This change is given by

$$d_{\mathrm{KS}}(\rho_\lambda,\rho_{\lambda_*}) = \sup_x\left|\rho_\lambda((-\infty,x]) - \rho_{\lambda_*}((-\infty,x])\right|, \tag{27}$$

and there are standard statistical tests for its significance.

For Eq. (1) and for a given δ, we considered hereafter the probability distribution ρ_δ of a simulated time series $h(t)$ sampled every year. The support of this probability measure is contained in the real line, more exactly is contained in the projection of the global attractor of the time-T map (with $T = 1$ yr) associated with Eq. (1). The simulations of $h(t)$ are each 85 000-yr long and have been performed over a δ-grid of size 6.6667×10^{-6} from $\delta = 0$ to $\delta = 16 \times 10^{-3}$.

Given an arbitrary reference parameter δ_0, with $\delta_0 = 13.3 \times 10^{-3}$ here, we computed $d_{\text{KS}}(\rho_{\delta_0}, \rho_\delta)$, where we used the kernel estimation algorithm of [BGK10] to estimate each probability measure ρ_δ. The numerical results are reported in Fig. 3. From these results, a sharp discontinuity—up to the numerical accuracy of our experiments—can be reasonably conjectured to take place for a critical parameter value δ_* lying between $\delta = 15.7 \times 10^{-3}$ and $\delta = 15.707 \times 10^{-3}$. As a consequence, a discontinuity in the CDF of the probability measure ρ_δ occurs.

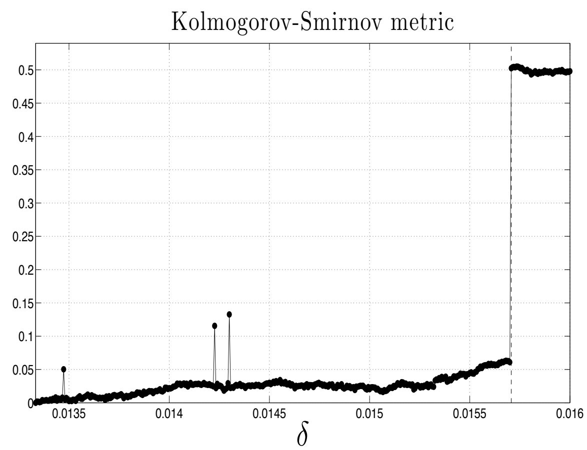

Fig. 3: **Sharp transition in the Kolmogorov-Smirnov (KS) metric.** The vertical dashed line emanates from the estimated value $15.7 \times 10^{-3} \le \delta_* \le 15.707 \times 10^{-3}$ at which a critical chaos-to-chaos transition occurs.

This approach based on the KS distance between one-dimensional CDFs is useful but it has its limitations. For instance, it does not allow one to distinguish what is happening dynamically right before and after the jump in the KS metric.

To get a better idea of the changes across δ_*, we examined carefully the time series $h(t)$ as the parameter δ is varied from $\delta < \delta_*$ in Fig. 4 to $\delta > \delta_*$ in Fig. 5. In Fig. 4, the most common year-to-year positive/negative excursions of h correspond to moderately warm (positive h anomaly, El Niño) and to moderately cold (negative h anomaly, La Niña) events. A small subset of these high and low excursions of h extend well beyond the typical range in Fig. 4, and are termed extreme El Niño and La Niña events.

As δ tends to δ_* from below, these extreme El Niño and La Niña events become less frequent; see the time series segments in panels (a) and (b) of Fig. 4). Such extremes disappear completely as δ_* is crossed, cf. Fig. 5.

The power spectral densities (PSDs) of the complete time series, though, as shown in Figs. 4 and 5, do not provide a clear imprint in the frequency domain of the the increasing rarity of occurrence of these extreme events as one approaches δ_* from below (Fig. 4), nor about the disappearance of the latter as the critical parameter δ_* has been crossed (Fig. 5).

We show in the next section that more plentiful and reliable information regarding the nature of the dynamical transition occurring at $\delta = \delta_*$ is gained by visualizing the corresponding PBA, as well as by estimating a statistical equilibrium μ_t that this PBA supports and that satisfies Eq. (20) for an appropriate choice of initial probability measure $\mathfrak{m}_0$.

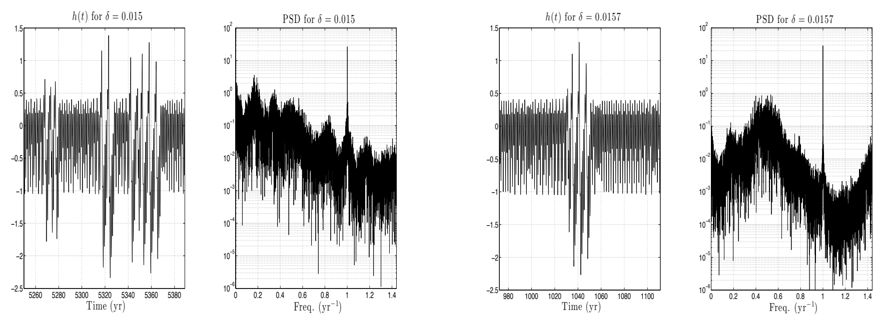

(a) **Time series and PSD**.
Here $a = 0.00630555$.

(b) **Time series and PSD**.
Here $a = 0.00630944$.

Fig. 4: **Time series and PSDs for $\delta = 15 \times 10^{-3}$ and $\delta = 15.7 \times 10^{-3}$.** Both these values of δ are strictly less than δ_*.

3.2 *Pullback symptoms*

The high-resolution numerical experiments in this section are designed to shed light on the transition in the behavior of the PBA and of the pullback statistical equilibrium μ_t it supports, as the parameter δ crosses the critical value δ_*.

To estimate μ_t as per (20), the initial histories are drawn from an initial distribution $\mathfrak{m}_0$ and propagated according to the RFDE (6). The distribution $\mathfrak{m}_0$ is designed as follows. Over the interval $[-\tau, 0]$, with $\tau = \tau_2 \approx 3.3$ yr, and for a grid resolution corresponding to n_g equally spaced points $\{\theta_j = -\tau(1 - j/n_g) : 1 \leq j \leq n_g\}$, the N initial histories ϕ_k are selected at random according to the formula

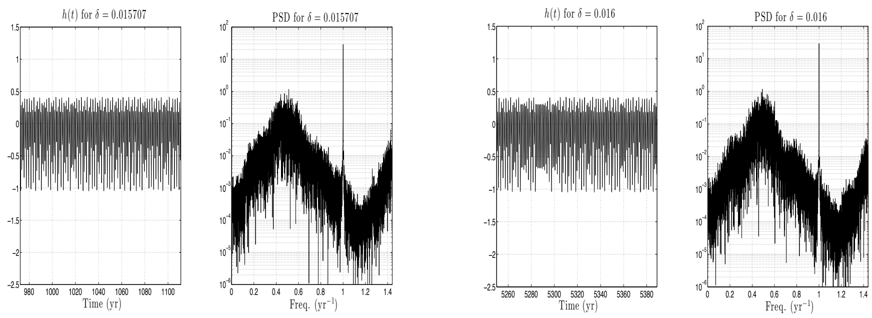

(a) **Time series and PSD**.
Here $a = 0.00630948$.

(b) **Time series and PSD**.
Here $a = 0.00631111$.

Fig. 5: **Time series and PSDs for** $\delta = 15.707 \times 10^{-3}$ **and** $\delta = 16 \times 10^{-3}$. Both these values of δ are strictly greater than δ_*

$$\phi_k(\theta_j) := -1 + \varepsilon k + (\varepsilon k)^{\frac{1}{p}} \xi_j, \;\; 1 \leq k \leq N, \tag{28}$$

with $\varepsilon = 2/N$ and $p \geq 1$. Here the ξ_j's are n_g independent real-valued random normal variables of mean zero and unit variance.

The fractional exponent $1/p$ in (28) is chosen so that the initial distribution follows roughly a Gaussian shape in the embedded $(\phi(-1), \phi(0))$-plane[9]: the closer this exponent is to unity, the sharper the peak of the distribution, and the smaller it is, the more bell-shaped the distribution. Figure 6 shows a distribution of $N = 4 \times 10^5$ initial histories.

Due to the dissipative effects present in Eq. (6), one does not need to reach exactly the asymptotic limit in (20) in order to obtain a reliable approximation of μ_t. For instance, after flowing from $s = 0$ to $t = t_* \approx 147.64$ yr, the $N = 4 \times 10^5$ initial histories whose distribution is shown in Fig. 6, one obtains the approximations of μ_t shown in Figs. 7 and 8. These approximations remain indistinguishable from those shown in these figures, when the same initial histories are flown from a time $s \ll 0$ up to the same t_* (not shown). Actually, even for some times $s > 0$, similar approximations (not shown) are obtained but we do not aim in this chapter to determine the minimum interval of time $t_* - s$ that ensures convergence in (20).

We focus here, as stated above, on the crisis of the global PBA and of its statistical equilibrium, when crossing the vertical dashed line in Fig. 3. For the sake of simplicity, we will no longer differentiate between μ_t and its approximations shown in Figs. 7 and 8.

Figures 7 and 8 clearly illustrate the singular nature of (the embedding of) μ_t with respect to the bell-shaped distribution $\mathfrak{m}_0$ shown in Fig. 6. This is not surprising, as the theory predicts that μ_t is supported by the strange PBA $\mathscr{A}_\delta(t)$, whose stretching and folding features were shown in Fig. 1 for $\delta = 15 \times 10^{-3}$. The PBA's strangeness is also manifest for the other values of δ in the interval $15.0 \times 10^{-3} \leq \delta \leq 15.707 \times$

[9] Here $\phi(-1)$ corresponds to the value of the initial histories at -1 yr.

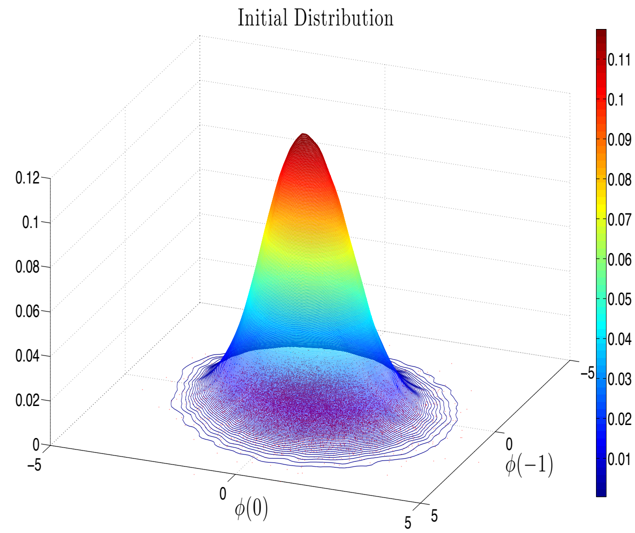

Fig. 6: **A distribution m_0 of initial histories, embedded in the $(\phi(-1), \phi(0))$-plane.** Here the initial histories are drawn according to (28) with $p = 12$ and $n_g = 400$.

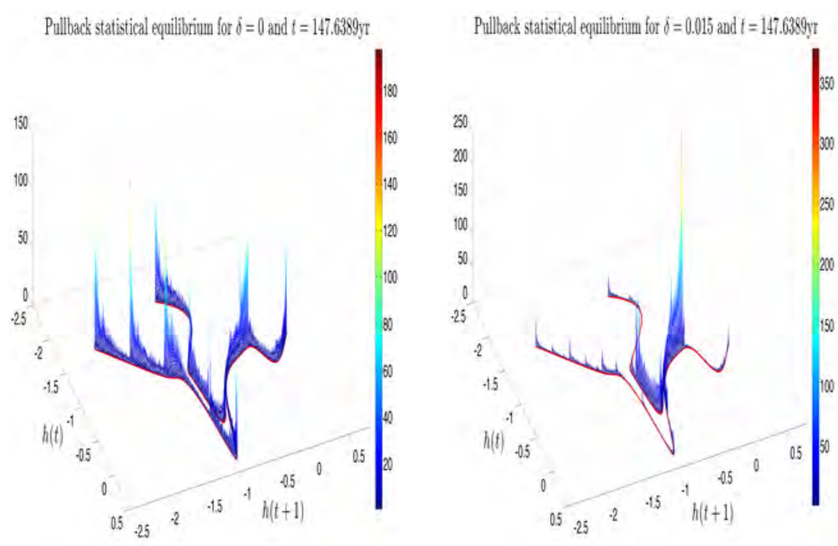

(a) $a = 0.00622222$. (b) $a = 0.00630555$.

Fig. 7: **Embedding of the pullback statistical equilibrium $\mu_t(\delta)$ associated with the DDE** (1). The embedding is shown within the $(h(t), h(t+1))$-plane, for $t \approx 147.64$ yr and for (a) $\delta = 0 < \delta_*$ and (b) $\delta = 15 \times 10^{-3} \lesssim \delta_*$ respectively.

10^{-3} (not shown), and the singular support of the probability measures $\mu_t(\delta)$ is plotted as red curves in Figs. 7(b) and 8(a,b).

Recall that what is observed here is within the embedded phase space $(h(t), h(t+1))$, and one may ask to which extent we can rely on this embedding to reach conclusions about the true nature of μ_t in the full phase space X. Rigorous results from the dimension theory of Borel probability measures with compact support [HK97] shed light on this issue. Denoting for a moment by $P\mu_t$ the projection of the measure μ_t onto the 2-D embedded phase space, like the one at hand, these results show that the correlation dimension D_2 [GP83] of the measure $P\mu_t$ visualized herein after embedding and projection[10] is:

$$D_2(P\mu_t) = \min(2, D_2(\mu_t)). \tag{29}$$

Therefore, if $D_2(P\mu_t)$ is strictly less than 2, we can conclude that the singular nature of this embedded measure—with respect to the Lebesgue measure of $\mathbb{R}^2$—reflects a genuinely singular nature of μ_t[11], and it is not due to some numerical artifact.

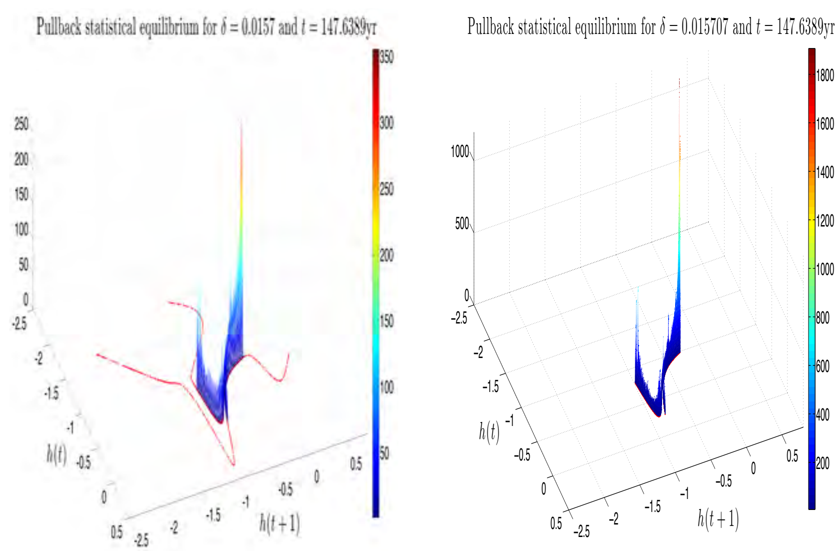

(a) $a = 0.00630944$. (b) $a = 0.00630948$.

Fig. 8: **Same as Fig. 7 but for (a)** $\delta = 15.7 \times 10^{-3} \lesssim \delta_*$ **and (b)** $\delta = 15.707 \times 10^{-3} \gtrsim \delta_*$.

We have estimated the correlation dimension $D_2(P\mu_t)$ following the algorithm of [GP04] and while taking into consideration the practical suggestions of [KS89]. We found that $D_2(P\mu_t) \approx 1.21$, which allows us to conclude that μ_t itself is singular,

[10] The "true" embedding dimension d given by the Takens embedding theorem may be greater than 2; see [Rob08] for a version of this theorem in the context of PBAs.

[11] with respect to the Lebesgue measure in $\mathbb{R}^d$.

and not just its 2-D embedding shown in Figs. 7 or 8. For brevity's sake, we will not distinguish hereafter between μ_t and its 2-D embedding.

Another important point apparent from inspection of Figs. 7 and 8 concerns a key difference between the statistical equilibrium μ_t for $\delta = 0$ in Fig. 7(a), located relatively far from the critical value δ_* at which the dynamical crisis occurs, and those shown for $\delta = 15 \times 10^{-3}$ in Fig. 7(b) and $\delta = 15.707 \times 10^{-3}$ in Fig. 8(a), located both closer to and still below δ_*. The latter two statistical equilibria do exhibit elongated filaments, like those in Fig. 7(a), but these filaments are much less populated by the nonlinear process than for the latter.

It follows that the statistical equilibrium μ_t supported by the PBA provides a global statistical description of the dynamics that is perfectly consistent with the observations reported at the end of Sect. 3.1 regarding the decrease in the rate of occurrence of extreme events as δ approaches δ_* from below. Indeed, the the latter decrease is manifested here by a reduction of the mass of μ_t that populates the elongated filaments, until its total disappearance when δ_* has been crossed, in Fig. 8(b).

In Fig. 8(b), the bulk of μ_t survives the crossing of δ_*, while the elongated filaments have disappeared altogether, i.e., no more of the extreme class of events survive. These numerical results confirm that the regions of the strange PBA that survive the crisis are those that are populated by the system's most probable states. A closer look at these regions show that they correspond to regions in which the PBA's foldings — like those shown in the inset of Fig. 1 — are the most robust to perturbations.

3.3 Dynamical interpretations

When the seasonal forcing is removed, i.e. $c = 0$ in Eq. (1), the ENSO model dynamics is periodic with a period T_δ, in years, that follows the empirical linear dependence

$$T_\delta = 8.7989 + 29.99(\delta - \delta_0), \tag{30}$$

throughout the interval $[\delta_0, 16 \times 10^{-3}]$ over which we performed the parameter dependence experiments reported in this chapter.

The characteristics of the underlying frequency-locked regimes between the internal oscillatory frequency $\omega_i = T_\delta^{-1}$ and the driving annual frequency ω_a, i.e. the integers p and q for which $\omega_i = \omega_a p/q$, depend thus on δ. Such a frequency-locked behavior takes place — in parameter space — in a so-called p/q-Arnold tongue [JBB84, JNG94, TSCJ94] whose δ-dependence makes it a p_δ/q_δ-Arnold tongue.

The ENSO model of DDE (1), subject to seasonal forcing and over the entire range of δ-values considered here, exhibits chaotic behavior, as described in Sect. 2.3. One can thus infer that, for each δ, chaos results from overlapping of a p_δ/q_δ-Arnold tongue with another, p'_δ/q'_δ-Arnold tongue [JBB84, Arn88].

The bifurcation theory of one-dimensional circle maps (e.g., [MK13, Chap. 7.4]), provides a possible explanation of the transition shown in Fig. 8, as δ is increased from $\delta = 15.7 \times 10^{-3}$ to $\delta = 15.707 \times 10^{-3}$. This theory addresses crises that occur within the overlap of two Arnold tongues, a region in which chaotic behavior occurs. Extrapolating to DDE models, such as the ENSO model investiagated herein, and adopting the language of PBAs, one could argue that the transition observed in Figs. 3 and 8 results from the coexistence of two strange PBAs at each fixed δ.

If such were the case, the two coexisting PBAs would correspond here to the one that lies within the square $[-1,0]^2$ of the $(h(t),h(t+1))$-plane and is shown by the red curve in Fig. 8(b), along with the one that exhibs filament extending out of this box and shown by the red curve in Fig. 8(a). In the present setting, the former is actually contained within the latter, but coexisting strange PBAs may, in general, be disjoint. If so, a crisis may still occur and manifest itself by a dynamics that hops between the two chaotic attractors, whether pullback or not, as one moves through parameter space; see [HHM+88, Fig. 6]. This phenomenon occurs whenever two Arnold tongues with nearby rotation numbers overlap, as certain crisis lines are crossed within the overlapping region; see [HHM+88, Fig. 2].

A complementary explanation of the transition observed here is provided by the theory of attractor widening [GORY87]: see [GORY87, Figs. 5 & 6] for a similar crisis in the case of the Ikeda map. Adopting again the language of PBAs, a collision between the PBA shown in Fig. 8(b) and an unstable periodic orbit would be responsible for initiating the crisis. To get the attractor widening, the collision would have to occur as δ crosses δ_* from above.

Whatever the exact explanation of the crisis, our study provides — to the best of the authors' knowledge — the first identification of such a crisis occurring in a delay differential model, as well as its first characterization in terms of PBAs and the statistical equilibria they support. We leave the more detailed and mathematically rigorous dynamical characterization of this crisis for another investigation, and turn next to a discussion of the impact of the noise on such a chaos-to-chaos crisis.

3.4 Crisis removal by small additive noise

One could argue that similar characterizations of the dynamical crisis discussed so far could have been inferred from the system's Poincaré map and the corresponding forward attractor. This is actually a valid argument for periodically forced systems, like the non-autonomous DDE at hand. For the case of a T-periodic system, a relationship between PBAs and a notion of forward attractor is known to exist and it does not even rely on Poincaré maps.

More precisely, the set $\widetilde{\mathscr{A}} = \bigcup_{t\in[0,T]} U(t,0)\mathscr{A}(0)$, where $\mathscr{A}(0)$ denotes the global PBA at time $t = 0$, satisfies, for any bounded set B of X, the following forward attraction property

$$\lim_{t\to+\infty} \sup_{\tau\in\mathbb{R}} \mathrm{dist}_X(U(\tau+t,t)B) = \widetilde{\mathscr{A}}. \tag{31}$$

We refer to [CLR13, Chap. 10.3] for a proof. The set $\widetilde{\mathscr{A}}$ is also known as a uniform forward global attractor, a concept introduced in [Har91], cf. also [CV02]; it is the minimal compact set of X that attracts all the trajectories—uniformly with respect to the initial time—that start from a bounded set; see [Har91, Chap. 8.3].

Nevertheless, the use of a standard Poincaré map or the concept of uniform attractor may hide, in the presence of noise, certain dynamical features that are revealed by a pullback approach that is not limited to the case of periodic or, more generally, deterministic non-autonomous forcing; see [GCS08, CSG11, Ghi17]. We illustrate hereafter this point in the context of the DDE model (1).

Let us thus consider the following stochastic modification of Eq. (1):

$$\mathrm{d}h = \left(aR\left[h\left(t-\frac{L}{2C_K}\right)\right] - bR\left[h\left(t-\frac{L}{C_K}-\frac{L}{2C_R}\right)\right] + c\cos(\omega_a t+\varphi)\right)\mathrm{d}t + \sigma\,\mathrm{d}W_t, \tag{32}$$

where W_t denotes a one-dimensional Brownian motion and $\sigma \geq 0$. This noise term in Eq. (32) is motivated by the presence of atmospheric high-frequency variability in the coupled climate system [KP94, JNG96, BNG97, EL97, KM97, RN00], a variability that is crudely represented herein by a white-noise process. A rigorous proof of the existence of random PBAs for such a non-autonomous stochastic DDE is beyond the scope of this chapter. We rely instead on numerical experiments to analyze the effects of noise on the inferred random PBA, as the parameter δ varies in a neighborhood of the critical value δ_* at which the chaos-to-chaos crisis occurs in the absence of noise.

Numerical results on the random PBA are shown in Figs. 9(a,b) for a noise intensity of $\sigma = 10^{-3}$, and the visual inspection of both panels strongly indicates that the chaos-to-chaos crisis did not survive the addition of small noise to the evolution equation. The results in Figs. 10(a,b) show, furthermore, that the corresponding pullback statistical equilibrium μ_t resembles the one obtained for $\delta = 0$ in the absence of noise, cf. Fig. 7(a). Dynamically, the crisis in the deterministic version of the model, for $\sigma = 0$, was associated with the disappearance of extreme El Niño and La Niña events as the critical parameter value δ_* is crossed from below. The addition of noise in the system triggers once again these extreme events, manifested by the expansion of the PBA in the embedded phase space, as evident when comparing the panels (b) of Figs. 8 and 10.

Complementary experiments performed for smaller values of the noise intensity σ have been conducted and have shown that this phenomenon is robust, while reducing the noise does result in extreme events becoming less and less probable. This is noticeable, for instance, by comparing the panels of Fig. 9 with those of Fig. 10, in which the noise level is $\sigma = 10^{-4}$, while the same noise realization was used in both figures.

The statistical equilibria shown in Figs. 10(a,b) resemble those in Fig. 7(b) for $\delta = 15\times 10^{-3}$, in which the main bulk of the density μ_t is located near the point $(-0.5,-1)$ in the $(h(t),h(t+1))$-plane, while the elongated PBA filaments — again

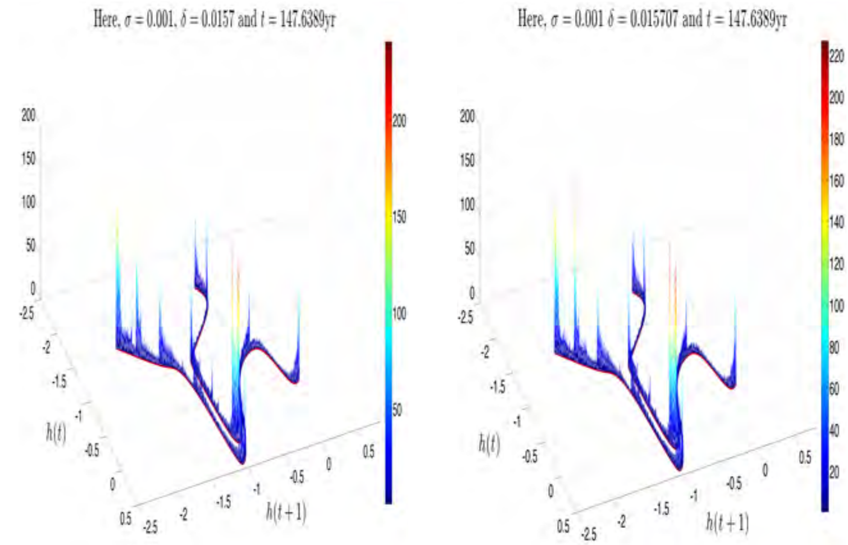

(a) $a = 0.00630944$. (b) $a = 0.00630948$.

Fig. 9: **Same as Fig. 8 but for the stochastic DDE** (32). The δ-values are again (a) $\delta = 15.7 \times 10^{-3}$ and (b) $\delta = 15.707 \times 10^{-3}$. The noise intensity $\sigma = 10^{-3}$ and the noise realization are the same for the panels (a) and (b), while the initial histories are again drawn from the distribution $\mathfrak{m}_0$ shown in Fig. 6.

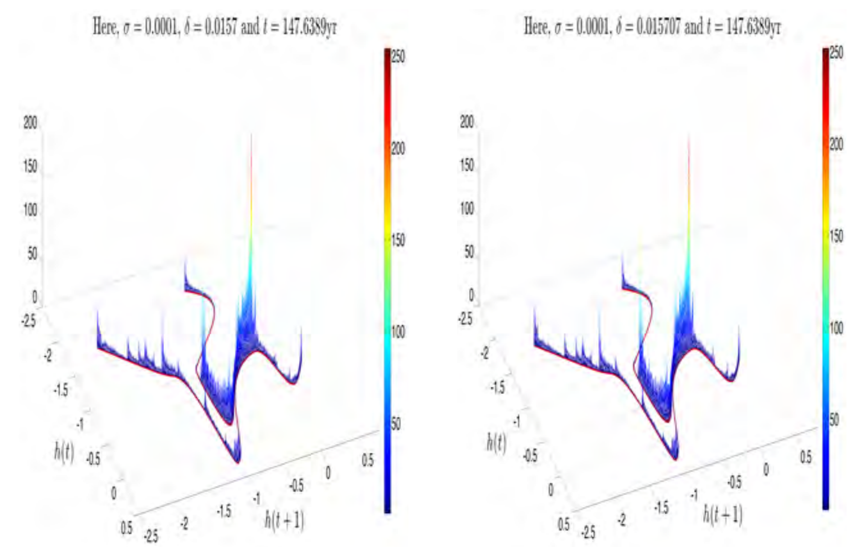

(a) $a = 0.00630944$. (b) $a = 0.00630948$.

Fig. 10: **Same as Fig. 9 but with much smaller noise, $\sigma = 10^{-4}$.**

like in (like in Fig. 7(b) — are less populated by the dynamics than for $\sigma = 10^{-3}$, i.e. the extreme events are less likely to occur.

This removal of the crisis by the addition of a small additive noise is actually consistent with noise effects, as shown for the fundamental circle map in [GCS08]. It was found there that a Devil's staircase step that corresponds to a rational rotation number can be "destroyed" by a sufficiently intense noise [GCS08, Appendix B]. In fact, the narrower a Devil's staircase steps is, the less robust is it to noise perturbations, while the wider ones are the most robust. Actually, the theory of topological equivalence in random dynamical systems — as analyzed in [Arn13, Con96, Con97] and as explained in [GCS08, Appendix B] — implies that the elimination of a Devil's staircase step, for a sufficient amount of noise, is manifested by the disappearance of a p/q-Arnold tongue. As a consequence, the corresponding asymptotic dynamics is no longer a periodic random attractor but a random fixed point.

Given this understanding of the smoothing effect of noise on the circle map's fine-grained resonant landscape, and the universal character of the circle map, one can deduce a heuristic result on the periodically forced DDE model considered here. To do so, recall the discussion of Sect. 3.3 about the dynamical origin of the chaos-to-chaos transition observed herein between $\delta = 15.7 \times 10^{-3}$ and $\delta = 15.707 \times 10^{-3}$, in the absence of noise; see again Figs. 3 and 8. Two dynamical mechanisms were proposed as potential causes of this transition.

In the case of the crossing of a crisis line within an overlap of two Arnold tongues [MK13], the removal of this crisis by the noise can be understood as the elimination of a nearby p/q-Arnold tongue; this elimnation, in turn, induces the disappearance of the coexisting chaotic attractor, as discussed in Sect. 3.3. Such an explanation is consistent, furthermore, with the resemblance between the PBAs shown in Figs. 9 and 10, on the one hand, with those shown in Fig. 7, on the other.

In the case of an attractor widening scenario, according to [GORY87], the noise would be responsible for jiggling an unstable periodic orbit that lies near the PBA $\mathscr{A}(t)$ so as to collide with the latter. Such a collision can cause an attractor widening to occur even for parameter values for which this unstable periodic orbit does not collide with $\mathscr{A}(t)$ in the absence of noise.

Whatever the mechanisms behind the chaos-to-chaos crisis of interest here, the way the noise enters the governing equations is crucial in causing the removal of the crisis or not. Typically, certain state-dependent noises may preserve the ordering between stationary solutions or between more complicated invariant sets [CPT16]. This ordering may, in turn, prevent the destruction of random periodic orbits and thus of p/q-Arnold tongues, as already pointed out in [GCS08, Appendix B]; such is the case, for instance, in the circle map, if the noise enters nonlinearly into the phase of the rotation. Likewise, a random unstable periodic orbit may stay away from the PBA in the case of certain multiplicative noises, a situation that may prevent an attractor widening scenario à la [GORY87] to be realized. The rigorous reduction techniques of [CLW15a, CLW15b], along with the approximation techniques of [CGLW16], provide a natural framework for analyzing the effects of state-dependent noise on DDE models such as Eq. (1) and they will be pursued elsewhere.

Acknowledgments

This work has been partially supported by the Office of Naval Research (ONR) Multidisciplinary University Research Initiative (MURI) grant N00014-12-1-0911 and N00014-16-1-2073 (MDC & MG), by the National Science Foundation grants OCE-1243175 (MDC & MG), DMS-1616981(MDC), and AGS-1540518 grant (JDN).

References

Arn88. V. I. Arnold, *Geometrical Methods in the Theory of Ordinary Differential Equations*, 2nd ed., Grundlehren der mathematischen Wissenschaften, vol. 250, Springer, 1988.

Arn13. L. Arnold, *Random Dynamical Systems*, Springer Science & Business Media, 2013.

BGK10. Z. I. Botev, J. F. Grotowski, and D. P. Kroese, *Kernel density estimation via diffusion*, The Annals of Statistics **38** (2010), no. 5, 2916–2957.

BH89. D. S. Battisti and A. C. Hirst, *Interannual variability in a tropical atmosphere–ocean model: Influence of the basic state, ocean geometry and nonlinearity*, Journal of the Atmospheric Sciences **46** (1989), no. 12, 1687–1712.

Bje69. J. Bjerknes, *Atmospheric teleconnections from the equatorial Pacific*, Monthly Weather Review **97** (1969), no. 3, 163–172.

BKT11. T. Bódai, G. Károlyi, and T. Tél, *A chaotically driven model climate: extreme events and snapshot attractors*, Nonl. Proc. Geophys. **18** (2011), no. 5, 573–580.

BKT13. ———, *Driving a conceptual model climate by different processes: Snapshot attractors and extreme events*, Phys. Rev. E **87** (2013), no. 2, 022822.

BNG97. B. Blanke, J. D. Neelin, and D. Gutzler, *Estimating the effects of stochastic wind stress forcing on ENSO irregularity*, J. Climate **10** (1997), 1473–1486.

BT12. T. Bódai and T. Tél, *Annual variability in a conceptual climate model: Snapshot attractors, hysteresis in extreme events, and climate sensitivity*, Chaos: An Interdisciplinary Journal of Nonlinear Science **22** (2012), no. 2, 023110.

Can86. Mark A Cane, *Experimental forecasts of el Niño*, Nature **321** (1986), 827–832.

CDF97. H. Crauel, A. Debussche, and F. Flandoli, *Random attractors*, Journal of Dynamics and Differential Equations **9** (1997), no. 2, 307–341.

CF94. H. Crauel and F. Flandoli, *Attractors for random dynamical systems*, Probability Theory and Related Fields **100** (1994), no. 3, 365–393.

CGH12. M. D. Chekroun and N. E. Glatt-Holtz, *Invariant measures for dissipative dynamical systems: Abstract results and applications*, Commun. Math. Phys. **316** (2012), no. 3, 723–761.

CGLW16. M. D. Chekroun, M. Ghil, H. Liu, and S. Wang, *Low-dimensional Galerkin approximations of nonlinear delay differential equations*, Disc. Cont. Dyn. Sys. A **36** (2016), no. 8, 4133–4177.

CKG11. M. D. Chekroun, D. Kondrashov, and M. Ghil, *Predicting stochastic systems by noise sampling, and application to the El Niño-Southern Oscillation*, Proc. Natl. Acad. Sci. USA **108** (2011), 11766–11771.

CLR01. T. Caraballo, J.A. Langa, and J.C. Robinson, *Attractors for differential equations with variable delays*, Journal of Mathematical Analysis and Applications **260** (2001), no. 2, 421–438.

CLR13. A. Carvalho, J. A. Langa, and J. Robinson, *Attractors for Infinite-Dimensional Non-autonomous Dynamical Systems*, Applied Mathematical Sciences, vol. 182, Springer, 2013.

CLW15a. M. D. Chekroun, H. Liu, and S. Wang, *Approximation of Stochastic Invariant Manifolds: Stochastic Manifolds for Nonlinear SPDEs I*, Springer Briefs in Mathematics, Springer, New York, 2015.

CLW15b. ______, *Parameterizing Manifolds and Non-Markovian Reduced Equations: Stochastic Manifolds for Nonlinear SPDEs II*, Springer Briefs in Mathematics, Springer, New York, 2015.

CMRV05. T Caraballo, P Marın-Rubio, and J Valero, *Autonomous and non-autonomous attractors for differential equations with delays*, Journal of Differential Equations **208** (2005), no. 1, 9–41.

CNK$^+$14. M. D. Chekroun, J. D. Neelin, D. Kondrashov, J. C. McWilliams, and M. Ghil, *Rough parameter dependence in climate models: The role of Ruelle-Pollicott resonances*, Proc. Natl. Acad. Sci. USA **111** (2014), no. 5, 1684–1690.

Con96. N. D. Cong, *Topological classification of linear hyperbolic cocycles*, Journal of Dynamics and Differential Equations **8** (1996), no. 3, 427–467.

Con97. N. D. Cong, *Topological Dynamics of Random Dynamical Systems*, Oxford University Press, 1997.

CPT16. M. D. Chekroun, E. Park, and R. Temam, *The Stampacchia maximum principle for stochastic partial differential equations and applications*, Journal of Differential Equations **260** (2016), no. 3, 2926–2972.

CSG11. M. D. Chekroun, E. Simonnet, and M. Ghil, *Stochastic climate dynamics: Random attractors and time-dependent invariant measures*, Physica D **240** (2011), no. 21, 1685–1700.

CTDN16. M. D. Chekroun, A. Tantet, H. A Dijkstra, and J. D. Neelin, *Mixing Spectrum in reduced phase spaces of stochastic differential equations. Part I: Theory*, submitted.

CV02. V. V. Chepyzhov and M. I. Vishik, *Attractors for Equations of Mathematical Physics*, vol. 49, Colloquium Publications, American Mathematical Society, 2002.

DBT15. G. Drótos, T. Bódai, and T. Tél, *Probabilistic concepts in a changing climate: A snapshot attractor picture*, J. Clim. **28** (2015), no. 8, 3275–3288.

DvGVLW95. O. Diekmann, S. A. van Gils, S. M. Verduyn Lunel, and H.-O. Walther, *Delay Equations: Functional, Complex, and Nonlinear Analysis*, Applied Mathematical Sciences, vol. 110, Springer-Verlag, New York, 1995.

EL97. Ch. Eckert and M. Latif, *Predictability of a stochastically forced hybrid coupled model of El Niño*, Journal of Climate **10** (1997), no. 7, 1488–1504.

ER85. J.-P. Eckmann and D. Ruelle, *Ergodic theory of chaos and strange attractors*, Rev. Modern Phys. **57** (1985), 617–656.

FMRT01. C. Foias, O. Manley, R. Rosa, and R. Temam, *Navier-Stokes Equations and Turbulence*, Encyclopedia of Mathematics and its Applications, vol. 83, Cambridge University Press, 2001.

GCS08. M. Ghil, M. D. Chekroun, and E. Simonnet, *Climate dynamics and fluid mechanics: Natural variability and related uncertainties*, Physica D **237** (2008), 2111–2126.

Ghi17. M. Ghil, *The wind-driven ocean circulation: Applying dynamical systems theory to a climate problem*, Discrete and Continuous Dynamical Systems-A **37** (2017), no. 1, 189–228.

GJ98. M. Ghil and N. Jiang, *Recent forecast skill for the El Niño/Southern Oscillation*, Geophys. Res. Lett. **25** (1998), no. 2, 171–174.

GORY87. C. Grebogi, E. Ott, F. Romeiras, and J. A. Yorke, *Critical exponents for crisis-induced intermittency*, Physical Review A **36** (1987), no. 11, 5365.

GP83. P. Grassberger and I. Procaccia, *Characterization of strange attractors*, Physical Review Letters **50** (1983), no. 5, 346.

GP04. ______, *Measuring the strangeness of strange attractors*, The Theory of Chaotic Attractors (B. R. Hunt, T.-Y. Tien-Yien Li, J. A. Kennedy, and H. E. Nusse, eds.), Springer, 2004, pp. 170–189.

GT00. E. Galanti and E. Tziperman, *Enso's phase locking to the seasonal cycle in the fast-sst, fast-wave, and mixed-mode regimes*, Journal of the Atmospheric Sciences **57** (2000), no. 17, 2936–2950.

GZ15. M. Ghil and I. Zaliapin, *Understanding ENSO variability and its extrema: A delay differential equation approach*, Observations, Modeling and Economics of Extreme Events (M. Ghil M. Chavez and J. Urrutia-Fucugauchi, eds.), Geophysical Monographs, vol. 214, American Geophysical Union & Wiley, 2015, pp. 63–78.

GZT08. M. Ghil, I. Zaliapin, and S. Thompson, *A delay differential model of ENSO variability: parametric instability and the distribution of extremes*, Nonlinear Processes in Geophysics **15** (2008), no. 3, 417–433.

Har91. A. Haraux, *Systèmes Dynamiques Dissipatifs et Applications*, vol. 17, Masson, Paris, 1991.

HHM$^+$88. T. Horita, H. Hata, H. Mori, T. Morita, K. Tomita, K. Shoichi, and H. Okamoto, *Local structures of chaotic attractors and q-phase transitions at attractor-merging crises in the sine-circle maps*, Progress of Theoretical Physics **80** (1988), no. 5, 793–808.

HK97. B. R. Hunt and V. Yu. Kaloshin, *How projections affect the dimension spectrum of fractal measures*, Nonlinearity **10** (1997), no. 5, 1031–1046.

HVL93. J. K. Hale and S. M. Verduyn-Lunel, *Introduction to Functional-Differential Equations*, Applied Mathematical Sciences, vol. 99, Springer-Verlag, New York, 1993.

JBB84. M. H. Jensen, P. Bak, and T. Bohr, *Transition to chaos by interaction of resonances in dissipative systems. I. Circle maps*, Physical Review A **30** (1984), no. 4, 1960.

JGN95. N. Jiang, M. Ghil, and D. Neelin, *Forecasts of equatorial Pacific SST anomalies by an autoregressive process using singular spectrum analysis*, Experimental Long-Lead Forecast Bulletin **4 (1)** (1995), 24–27.

JN93. F.-F. Jin and J. D. Neelin, *Modes of interannual tropical ocean-atmosphere interaction-A unified view. Part III: Analytical results in fully coupled cases*, Journal of the Atmospheric Sciences **50** (1993), no. 21, 3523–3540.

JNG94. F.-F. Jin, J. D. Neelin, and M. Ghil, *El Niño on the Devil's Staircase: Annual subharmonic steps to chaos*, Science **274** (1994), 70–72.

JNG96. F.-F. Jin, J. D. Neelin, and M. Ghil, *El Niño/Southern Oscillation and the annual cycle: Subharmonic frequency locking and aperiodicity*, Physica D **98** (1996), 442–465.

KCG15. D. Kondrashov, M. D. Chekroun, and M. Ghil, *Data-driven non-Markovian closure models*, Physica D: Nonlinear Phenomena **297** (2015), 33–55.

KCRG13. D. Kondrashov, M. D. Chekroun, A. W. Robertson, and M. Ghil, *Low-order stochastic model and "past-noise forecasting" of the Madden-Julian Oscillation*, Geophys. Res. Lett. **40** (2013), 5305–5310, doi:10.1002/grl.50991.

Kel75. John L Kelley, *General Topology*, Springer Science & Business Media, 1975.

KKP15. A. Keane, B. Krauskopf, and C. Postlethwaite, *Delayed feedback versus seasonal forcing: Resonance phenomena in an El Niño Southern Oscillation model*, SIAM Journal on Applied Dynamical Systems **14** (2015), no. 3, 1229–1257.

KKP16. ———, *Investigating irregular behavior in a model for the El Niño Southern Oscillation with positive and negative delayed feedback*, SIAM Journal on Applied Dynamical Systems **15** (2016), no. 3.

KM97. R. Kleeman and A. M. Moore, *A theory for the limitation of ENSO predictability due to stochastic atmospheric transients*, Journal of the Atmospheric Sciences **54** (1997), no. 6, 753–767.

KP94. R. Kleeman and S.B. Power, *Limits to predictability in a coupled ocean-atmosphere model due to atmospheric noise*, Tellus A **46** (1994), no. 4, 529–540.

KS89. E.J. Kostelich and H. L. Swinney, *Practical considerations in estimating dimension from time series data*, Physica Scripta **40** (1989), no. 3, 436.

KS14. B. Krauskopf and J. Sieber, *Bifurcation analysis of delay-induced resonances of the El-Niño Southern Oscillation*, Proc. R. Soc. A (M. Ghil, M.D. Chekroun, and G. Stepan, eds.), vol. 470, The Royal Society, 2014, p. 20140348.

LR14. G. Lukaszewicz and J.C. Robinson, *Invariant measures for non-autonomous dissipative dynamical systems*, Disc. Cont. Dyn. Sys. A **34** (2014), no. 10, 4211–4222.

LWY13. K. Lu, Q. Wang, and L.-S. Young, *Strange attractors for periodically forced parabolic equations*, vol. 224, Memoirs of the American Mathematical Society, no. 1054, American Mathematical Society, Providence, RI, 2013.

MCZ91. M. Münnich, M.A. Cane, and S.E. Zebiak, *A study of self-excited oscillations of the tropical ocean-atmosphere system. Part II: Nonlinear cases*, Journal of the atmospheric sciences **48** (1991), no. 10, 1238–1248.

MK13. H. Mori and Y. Kuramoto, *Dissipative Structures and Chaos*, Springer, 2013.

MNY03. C. R. Mechoso, J. D. Neelin, and J.-Y. Yu, *Testing simple models of ENSO*, J. Atmos. Sci. **60** (2003), 305–318.

NBH$^+$98. J. D. Neelin, D. S. Battisti, A. C. Hirst, F.-F. Jin, Y. Wakata, T. Yamagata, and S. E. Zebiak, *ENSO theory*, Journal of Geophysical Research: Oceans (1978–2012) **103** (1998), no. C7, 14261–14290.

NJS00. J. D. Neelin, F.-F. Jin, and H.-H. Syu, *Variations in ENSO phase-locking*, J. Climate **13** (2000), 2570–2590.

PGC16. S. Pierini, M. Ghil, and M.D. Chekroun, *Exploring the pullback attractors of a low-order quasigeostrophic ocean model: The deterministic case*, Journal of Climate **29** (2016), no. 11, 4185–4202.

Phi92. S. G. H. Philander, *El Niño, La Niña, and the Southern Oscillation*, Academic Press, San Diego, 1992.

RGO90. F.J. Romeiras, C. Grebogi, and E. Ott, *Multifractal properties of snapshot attractors of random maps*, Physical Review A **41** (1990), no. 2, 784.

RN00. M. S. Roulston and J. D. Neelin, *The response of an ENSO model to climate noise, weather noise and intraseasonal forcing*, Geophys. Res. Lett. **27** (2000), 3723–3726.

Rob08. J.C. Robinson, *A topological time-delay embedding theorem for infinite-dimensional cocycle dynamical systems*, Discrete and Continuous Dynamical Systems. Series B **9** (2008), no. 3-4, 731–741.

Rue99. D. Ruelle, *Smooth dynamics and new theoretical ideas in nonequilibrium statistical mechanics*, Journal of Statistical Physics **95** (1999), no. 1, 393–468.

SS88. Max J Suarez and Paul S Schopf, *A delayed action oscillator for ENSO*, Journal of the atmospheric Sciences **45** (1988), no. 21, 3283–3287.

Tak81. F. Takens, *Detecting strange attractors in turbulence*, Dynamical Systems and Turbulence, Warwick 1980, Springer, 1981, pp. 366–381.

TCZ95. E. Tziperman, M.A. Cane, and S. E. Zebiak, *Irregularity and locking to the seasonal cycle in an ENSO prediction model as explained by the quasi-periodicity route to chaos*, Journal of the Atmospheric Sciences **52** (1995), no. 3, 293–306.

Tem97. R. Temam, *Infinite-Dimensional Dynamical Systems in Mechanics and Physics*, 2nd ed., Applied Mathematical Sciences, vol. 68, Springer-Verlag, New York, 1997.

TSCJ94. E. Tziperman, L. Stone, M.A. Cane, and H. Jarosh, *El Niño chaos: Overlapping of resonances between the seasonal cycle and the Pacific ocean-atmosphere oscillator*, Science **264** (1994), no. 5155, 72–74.

WY01. Q. Wang and L.-S. Young, *Strange attractors with one direction of instability*, Communications in Mathematical Physics **218** (2001), no. 1, 1–97.

WY03. ———, *Strange attractors in periodically-kicked limit cycles and Hopf bifurcations*, Communications in Mathematical Physics **240** (2003), no. 3, 509–529.

WY08. ———, *Toward a theory of rank one attractors*, Annals of Mathematics (2008), 349–480.

You16. L.-S. Young, *Generalizations of SRB measures to nonautonomous, random, and infinite dimensional systems*, Journal of Statistical Physics **166** (2016).